Electronic Supplementary Material (ESI) for Journal of Materials Chemistry A.

Supporting Information

A facile route to fabricate double atoms catalysts with controllable atomic spacing for r-WGS reaction

Hongyu Chen,[a] Ying Zhang,[b] Qian He,[a] Hao Zhang,[b] Sheng Xu,[b] Xiaohui He[a,]*, Hongbing Ji,[a,b,c,]*

[a] Fine Chemical Industry Research Institute, School of Chemistry, Sun Yat-sen University, Guangzhou 510275, China

[b] Fine Chemical Industry Research Institute, School of Chemical Engineering and Technology, Sun Yat-sen University, Zhuhai 519082, China

[c] School of Chemical Engineering, Guangdong University of Petrochemical Technology, Maoming 525000, China

*Correspondence: jihb@mail.sysu.edu.cn; hexiaohui@mail.sysu.edu.cn

List of content

Materials and general methods

The benzene-1,3-dicarbaldehyde (*CAS no*. 626-19-7), 2,2',2''-triaminotris(ethylamine) (Tren, *CAS no*. 4097-89-6), potassium borohydride (*CAS no*. 13762-51-1), nickel(II) Chloride (*CAS no*. 7718-54-9), nickel(II) perchlorate hexahydrate (*CAS no*. 13520-61-1), cobalt(II) perchlorate hexahydrate (*CAS no*. 13478-33-6) and bis(diphenylphosphine)ferrocene metal complexes ($NiCl_2$dppf, *CAS no*. 67292-34-6; $PdCl_2$dppf, *CAS no*. 72287-26-4) were purchased from **Sigma-Aldrich**. The 2-pyridinecarboxaldehyde (*CAS no*. 1121-60-4), triacetoxyborohydride (*CAS no*. 56553-60-7), di-(2-picolyl) amine (*CAS no*. 1539-42-0), 70 % perchloric acid (*CAS no*. 7601-90-3), sodium bicarbonate (*CAS no*. 144-55-8), sodium carbonate (*CAS no*. 497-19-8) and all solvents (analytical purity) were purchased from **Energy Chemical**. The carbon black (*CAS no*. 1333-86-4) was purchased from **Alfa Aesar**. All the reagents and solvents are used without any purification unless anhydrous condition was noted. All reactions are performed in a flame-dried glassware under nitrogen atmosphere except when aqueous solution was needed as reagents. ESI-HRMS were recorded on a Waters Xevo Q-TOF MS and a Thermofisher LTQ Orbitrap Elite MS. 200-300 mesh silica gel was used for flash chromatography and was produced by Qingdao Marine Chemical Industrials. TLC and pre-TLC were carried out on precoated silica gel GF254 plates (Yantai Chemical Industrials) and the TLC spots were viewed at 254 nm. X-ray crystallographic analysis was carried out on a Agilent SuperNova, Dual, Cu at zero, AtlasS2 diffractometer with graphite monochromated Mo Kα radiation (λ = 0.71073 Å). The metal loadings were determined by ICP-OES on a PerkinElmer OPTIMA 8000DV and EA on Vario EL cube instrument, respectively. BET surface areas were measured on a Micromeritic ASAP2020M analyzer at liquid nitrogen temperature with pre-evacuation at 200 °C for 6 h. Specific surface areas were estimated based on the BET equation. PXRD patterns were recorded on a Bruker D8 Advanced diffractometer. The images of TEM and STEM were obtained on a FEI Tecnai G2 F30 operated at 300 kV. AC HAADF-STEM images and elemental analysis mapping were obtained on a JEM ARM200F transmission electron microscopy operated at 200 kV, which is incorporated with double spherical aberration correctors. Catalytic tests of r-WGS reaction were carried out in a vertical continuous-flow fixed-bed quartz reactor with inner diameter of 7 mm at atmospheric pressure and quantified by online gas chromatography (GC 7890II, Techcomp. China Ltd) with a molecular sieve (TDX-01) packed column and thermal conductivity detector (TCD). The in situ mass spectrometry traces for products of r-WGS reactions were obtained on the Hiden Analytical HPR-20 QIC benchtop Gas Analysis System. The X-ray absorption spectroscopy (XAS) measurements for the Ni K-edge were performed in fluorescence mode on beamline 20-BM-B in the Advanced Photon Source at Argonne National Laboratory. Ni foil was used as reference sample and measured in transmission mode. The precursors, dinuclear nickel cryptate [S1] dinuclear cobalt cryptate [S2] and $NiCl_2$(TPA) [S3] were synthesized and characterized as previous reports.

X-ray Crystal Data for dinuclear nickel cryptate

Chemical formula	$C_{37}H_{57}Cl_3N_8Ni_2O_{12}$
mw	1029.67
Crystal system, space group	monoclinic, $P2_1/c$
Temperature (K)	293(2)
a, b, c (Å)	17.0815 (7), 15.8476 (5), 19.4081 (9)
α, β, γ (°)	90, 114.942 (5), 90
V (Å^3)	4763.8 (4)
Z	4
Radiation	Mo $K\alpha$ (λ = 0.71073 Å)
μ (mm^{-1})	1.023
Crystal size (mm)	0.20 × 0.20 × 0.20
Diffractometer	SuperNova, Dual, Cu at zero, AtlasS2
F (000)	2112.0
ρ_{calc} g/cm^3	44200, 22112, 18569
2Θ range for data collection/°	6.622 to 60.676
Goodness-of-fit on F^2	1.024
Final R indexes [I>=2σ (I)]	R_1=0.0486, wR_2=0.1040
Final R indexes [all data]	R_1=0.0730, wR_2=0.1179

A clear, blue block specimen of dinuclear nickel cryptate was obtained from MeCN/Et_2O. Crystal data were obtained on a SuperNova, Dual, Cu at zero, AtlasS2 diffractometer employing graphite monochromated Mo $K\alpha$ radiation (λ = 0.71073 Å) at 293(2) K and operating in the multi-scan mode. The structure was solved by direct methods using Olex2[S4] and refined with full-matrix least-squares calculations on F^2 using SHELXL-2018/3[S5]. Owing to the cavity structure of dinuclear nickel cryptate, there were heavily disordered solvent molecules (MeCN/Et_2O) that could not be identified from different Fourier map. Accordingly, the SQUEEZE routine of PLATON[S6] was applied to remove the contributions to the scattering from the solvents. All non-hydrogen atoms were refined anisotropically. The hydrogen atom positions were geometrically idealized and allowed to ride on their parent atoms. Crystallographic data for dinuclear nickel cryptate have been deposited at the Cambridge Crystallographic Data Centre (deposition no. CCDC 1957731). Copies of these data can be obtained free of charge via www.ccdc.cam.ac.uk/conts/retrieving. html

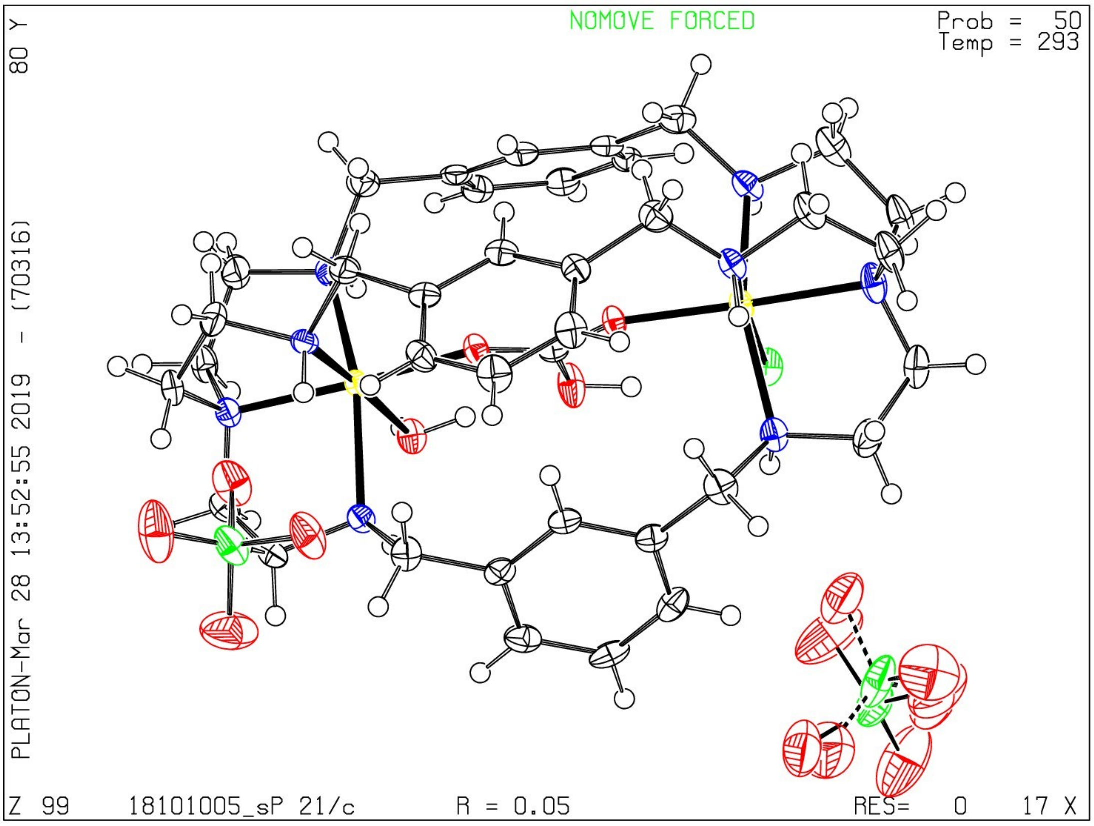

Figure S1. X-ray crystal structure for dinuclear nickel cryptate

Synthetic procedure of metal complexes

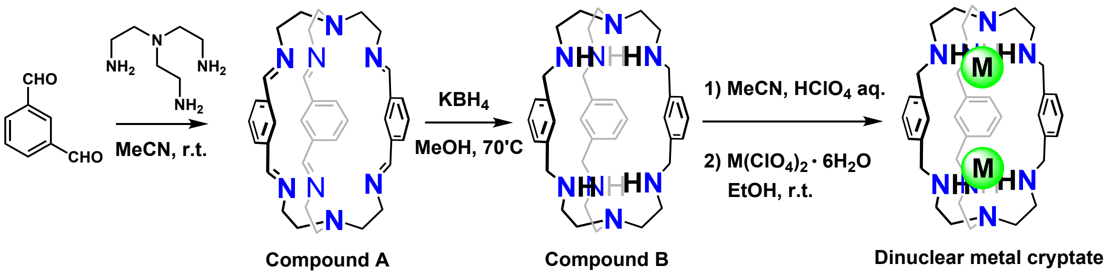

Compound A.[S1] To a solution of 2,2’,2’’-triaminotris(ethylamine) (1.096 g, 7.5 mmol) in MeCN (60 mL) was slowly added Benzene-1,3-dicarbaldehyde (0.036 M in MeCN, 300 mL, 10.8 mmol) at room temperature within 3 hours. Then, the mixture was stirred at room temperature for another 12 h, and the white precipitate would slowly appear. After completely removing the solvent by filtration, the white precipitate was first washed with a small portion of MeCN, and then carefully dried under vacuum at R.T. to give 1.73 g compound A as pale-yellow solid. Yield: 82.0 %. ^{1}H-NMR (600 MHz, $CDCl_3$)：δ 8.19 (dd, J = 7.7, 1.5 Hz, 6H), 7.58 (s, 6H), 7.53 (t, J = 7.7 Hz, 3H), 5.33 (s, 3H), 3.78 (s, 6H), 3.28 (s, 6H), 2.94 (s, 6H), 2.69 (s, 6H).

Compound B. [S1] To a suspension of compound A (1.878 g, 3.2 mmol) in anhydrous methanol (50 mL), potassium borohydride (2.0 g, 37.1 mmol) was slowly added at R.T.. The mixture was then stirred and refluxed overnight under inert atmosphere to ensure the reduction was completed. (**Caution!** This reduction step may generate hydrogen gas. Please be careful in a large scale.) The solvent was subsequently removed under vacuum. The residue was suspended in 2 M NH_4Cl aqueous solution (120 mL) and the aqueous phase was extracted with dichloromethane (6 × 40 mL). The combined organic layers were washed by brine and then water, dried over Na_2SO_4 and vaporized to a quarter volume. The concentrated solution was slowly added into anhydrous Et_2O to give a white precipitate. After quick filtration and drying treatment under vacuum, 1.40 g compound B was obtained as a deliquescent and white solid. Yield: 73.1 %. (If there was water remained, compound B would be very viscous.)^{1}H-NMR (600 MHz, $CDCl_3$, TMS)：δ 7.24-7.10 (m, 12H), 3.62 (s, 12H), 2.66 (t, J = 5.2 Hz, 12H), 2.58 (t, J = 5.3 Hz, 12H). ESI-HRMS *m/z* 300.2312 $[M+2H]^{2+}$ (calcd. for $C_{36}H_{56}N_8$ $[M+2H]^{2+}$ 300.2311), 599.4539 $[M+H]^+$ (calcd. for $C_{36}H_{55}N_8$ $[M+H]^+$ 599.4528)

Dinuclear nickel cryptate [S1] To a suspension of compound B (310 mg, 0.52 mmol) in MeCN (4 mL), the $HClO_4$ aqueous solution (4.95 mmol/L, 1 mL) was added and sonicated for 20 mins to form a clear solution. Then ethanol (20 mL) was added and stirred for another 10 mins before the addition of sodium bicarbonate aqueous solution (417 mg in 4 mL water). The mixture was stirred for 5 mins, and the solution of nickel(II) perchlorate hexahydrate (502 mg in 4 mL ethanol) was added slowly to form a blue suspension. The suspension was stirred for another 24h before filtration. The blue precipitate was washed by a portion of ethanol and dichloromethane, then dried under vacuum at R.T. to give 429 mg dinuclear nickel cryptate as the pale-blue solid. Yield:85.0 %. ESI-HRMS *m/z* 387.1516 (calcd. For $C_{37}H_{54}N_8Ni_2O_3$ $[M]^{2+}$ 387.1502)

Dinuclear cobalt cryptate [S2] The synthetic procedure of dinuclear cobalt cryptate was the same as the corresponding nickel complex. Yield:81.2 %. ESI-HRMS *m/z* 388.1489 (calcd. For $C_{37}H_{54}N_8Co_2O_3$ $[M]^{2+}$ 388.1486)

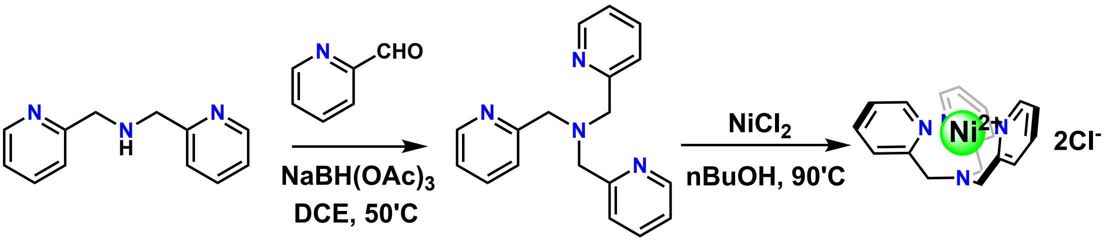

TPA

NiCl$_2$TPA

Tris(2-pyridyl)methylamine (TPA) [S3] Both of 2-pyridinecarboxaldehyde (0.58 g, 5.38 mmol) and di-(2-picolyl) amine (0.98 g, 4.91 mmol) were first dissolved in anhydrous 1,2-dichloroethane (20 mL), and then sodium triacetoxyborohydride (1.66 g, 7.85 mmol) was added into the solution. The mixture was heated to 50 ℃ stirred for 2 days under N_2 atmosphere. The solvent was removed under vacuum and the resulted crude product was dissolved in 20 mL of dichloromethane, washed twice with saturated Na_2CO_3 aqueous solution. The organic layer was concentrated under vacuum and the resulted yellow oil was further purified by column chromatography on alumina (ethyl acetate as eluent) to yield 710 mg TPA as yellowish solid. Yield: 50.0 %. ^{1}H-NMR (600 MHz, $CDCl_3$)：δ 8.53 (dd, *J* = 4.8, 1.5 Hz, 3H), 7.65 (tt, *J* = 7.7, 1.5 Hz, 3H), 7.57 (d, *J* = 7.8 Hz, 3H), 7.14 (d, *J* = 6.0 Hz, 3H), 3.91 (s, 6H).

NiCl$_2$TPA [S3] To a solution of TPA (100 mg, 0.34 mmol) in n-Butanol (5 mL), a sonicated suspension of $NiCl_2$ (40.2 mg, 0.31 mmol) in n-Butanol (8 mL) was added under N_2 stream. The mixture was heated to 90 ℃ for 1h under N_2 atmosphere. The solvent was then removed under vacuum, and n-hexane (10 mL) was added into the residue and stayed overnight. After completely removing the solvent by filtration, the blue precipitate was first washed with a small portion of n-hexane, and then dried under vacuum at R.T. to give 105 mg NiCl$_2$TPA as the blue solid. Yield: 73.5 %. ESI-HRMS *m/z* 174.0426 (calcd. For $C_{18}H_{18}N_4Ni$ $[M]^{2+}$ 174.0437)

Typical synthetic procedure of catalysts by dry ball milling

Ni_2/N-C was taken as example to show the preparation process. A mixture of as-prepared dinuclear nickel cryptate and carbon black with the metal weight ratio of 1:1000 (i.e. 11.7 mg and 1.5 g, respectively) was added to a commercially available agate jar (50 mL) with 30 g agate grinding balls (Φ6 mm in diameter). Then two agate jars with mixture were placed in a planetary ball mill (CHISHUN, QM3SP2), and the mixture were milled for 24 h at 400 r/min. Afterwards, the milled mixture was pyrolyzed at 600 °C for 2 h under flowing N_2 atmosphere with a heating rate of 3 °C/min, and Ni_2/N-C was obtained. Other catalysts, including Co_2/N-C and single-atom Ni_1/N-C were prepared with the same synthetic procedure. Heteronuclear catalysts including Fe_1Pd_1/N-C and Fe_1Ni_1/N-C were prepared by the same procedure with an additional urea as nitrogen source (the weight ratio of urea and carbon black was 1:1). The reference catalyst, N-C, was prepared by the same procedure with the metal-free cryptate ligand as the precursor.

Synthesis of Ni NPs/N-C

The bis(η5-2,4-cyclopentadien-1-yl) nickel (800 mg) was first dissolved in 15 mL dichloromethane under ultrasound. Then the carbon black (500 mg) and urea (100 mg) were added slowly and stirred for 15 min before dried at 80 °C. Afterwards, the mixture was pyrolyzed at 600 °C for 2 h under flowing N_2 atmosphere with a heating rate of 3 °C/min, and Ni NPs/N-C was obtained. The Ni loading of prepared Ni NPs/N-C catalyst was 6.8 wt.% determined by ICP-OES analysis and characterized by STEM and PXRD experiments. The average sizes of metal particles and their size distributions were obtained as 14 ± 1.5 nm by averaging at least 100 particles randomly distributed in the STEM images.

Synthesis of the reference catalyst Ni powders

The reduction of NiO powders was carried out in a vertical continuous-flow fixed-bed quartz reactor with inner diameter of 7 mm at atmospheric pressure. 20.0 mg NiO powders of catalysts were held at the center of the reactor with quartz-wool plugs. The flow rates of 20% H_2/He purging of the sample tube was kept at 20 standard cm^3 per minute. After the temperature stabilizing at 773 K, the sample was reduced for five hours before test.

Characterizations of catalysts

Table S1. Metal contents and BET areas for catalysts

Catalysts	**Metal contents (wt.%)**	**S_{BET} (m^2/g)**	**Pore volume (cm^3/g)**	**Average pore size (nm)**
Ni_2/N-C	0.09	124.7	0.40	12.9
Ni_1/N-C	0.1	98.9	0.38	17.5
Co_2/N-C	0.06	146.6	0.21	5.9
Fe_1Pd_1/N-C	Fe(0.03), Pd(0.06)	142.5	0.46	12.8
Fe_1Ni_1/N -C	Fe(0.06), Ni(0.09)	141.1	0.45	12.8

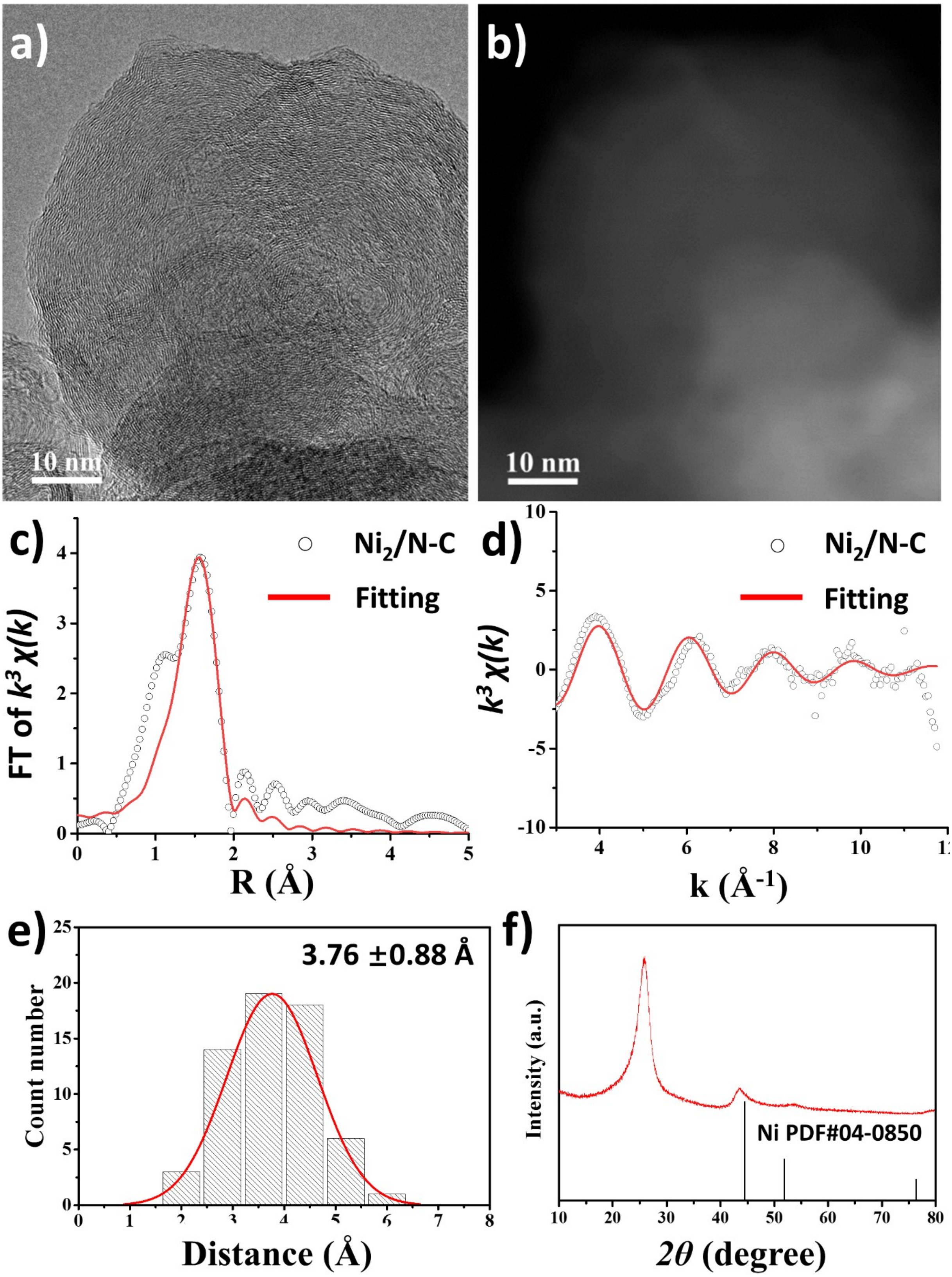

Figure S2. (a) TEM image; (b) STEM image; (c,d) EXAFS fitting results of Ni K-edge at R and k space, respectively; (e) the average distances of pairwise Ni atoms and their distributions by averaging at least 60 pairs of Ni atoms randomly distributed in the ac HAADF-STEM images; (f) PXRD patterns of Ni_2/N-C.

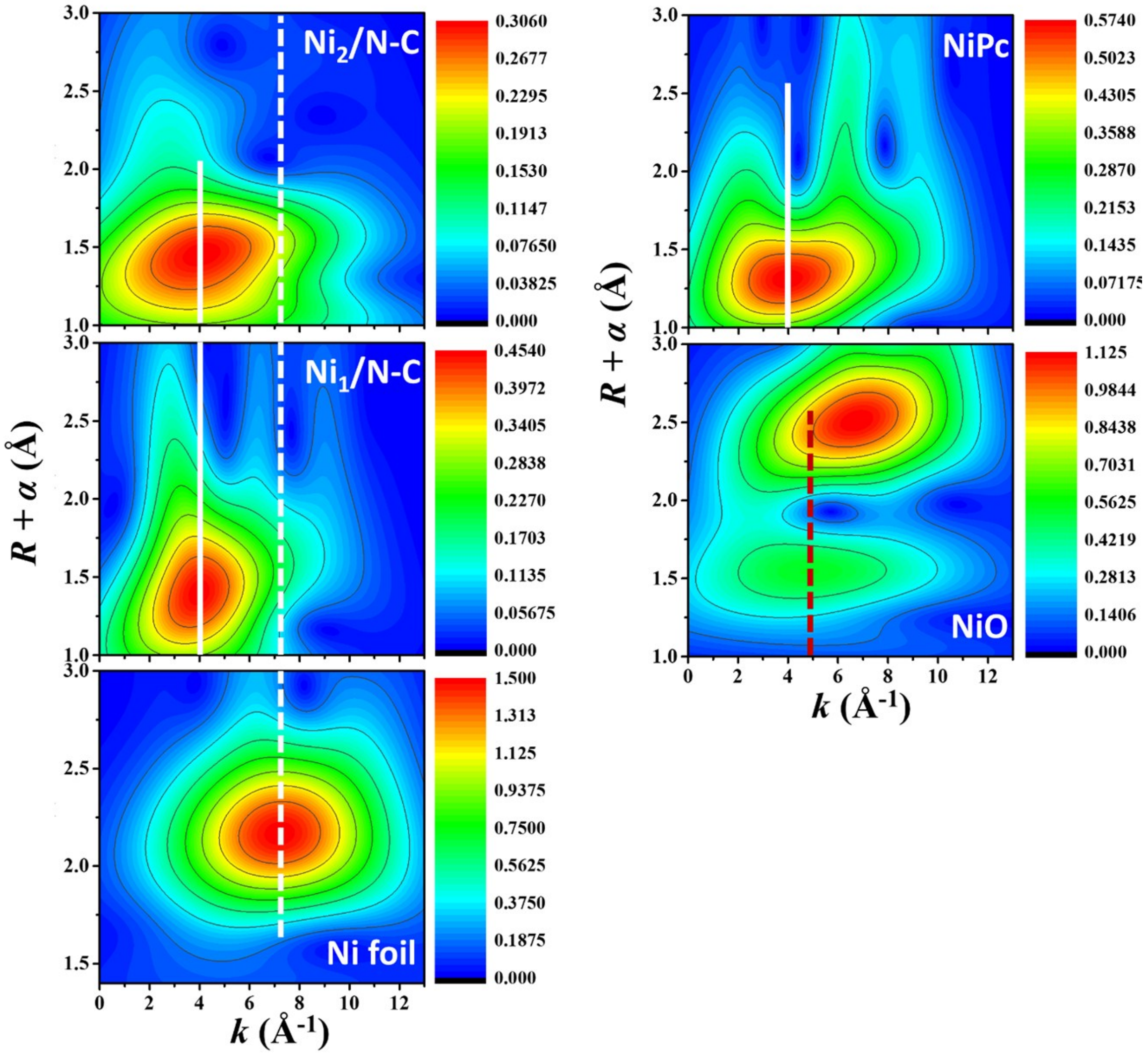

Figure S3. Wavelet transform (WT) Ni K-edge EXAFS spectra of Ni$_2$/N-C, Ni$_1$/N-C, Ni foil, NiPc and NiO.

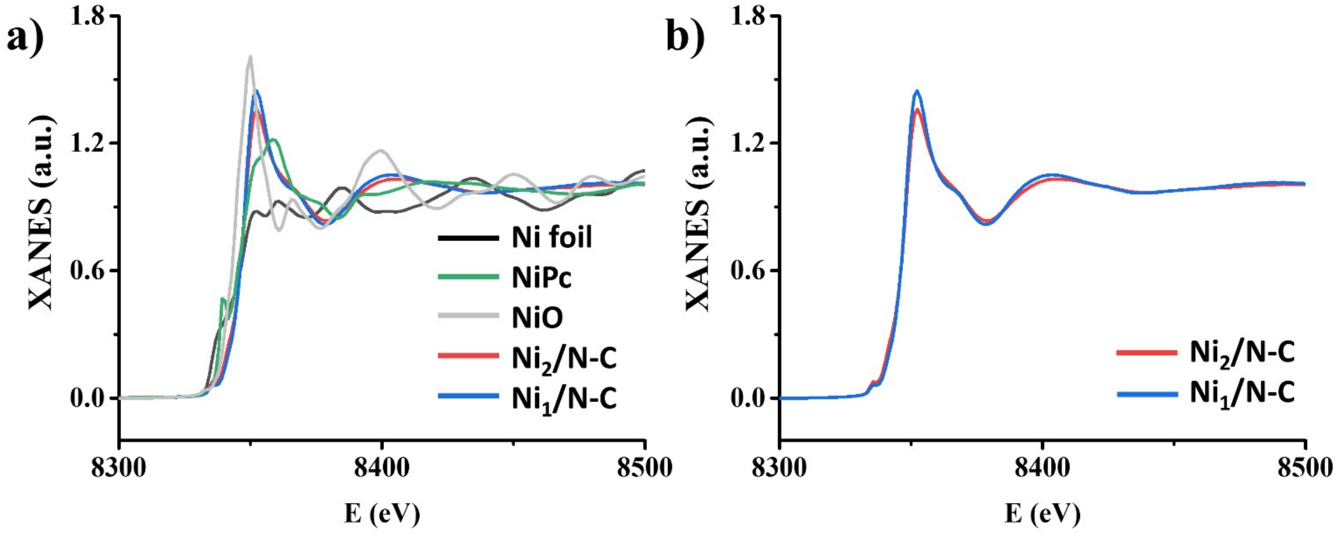

Figure S4. (a) Ni K-edge XANES spectra of Ni$_2$/N-C, Ni$_1$/N-C and references; (b) Ni K-edge XANES spectra of Ni$_2$/N-C and Ni$_1$/N-C, clearly showing the similar near-edge features.

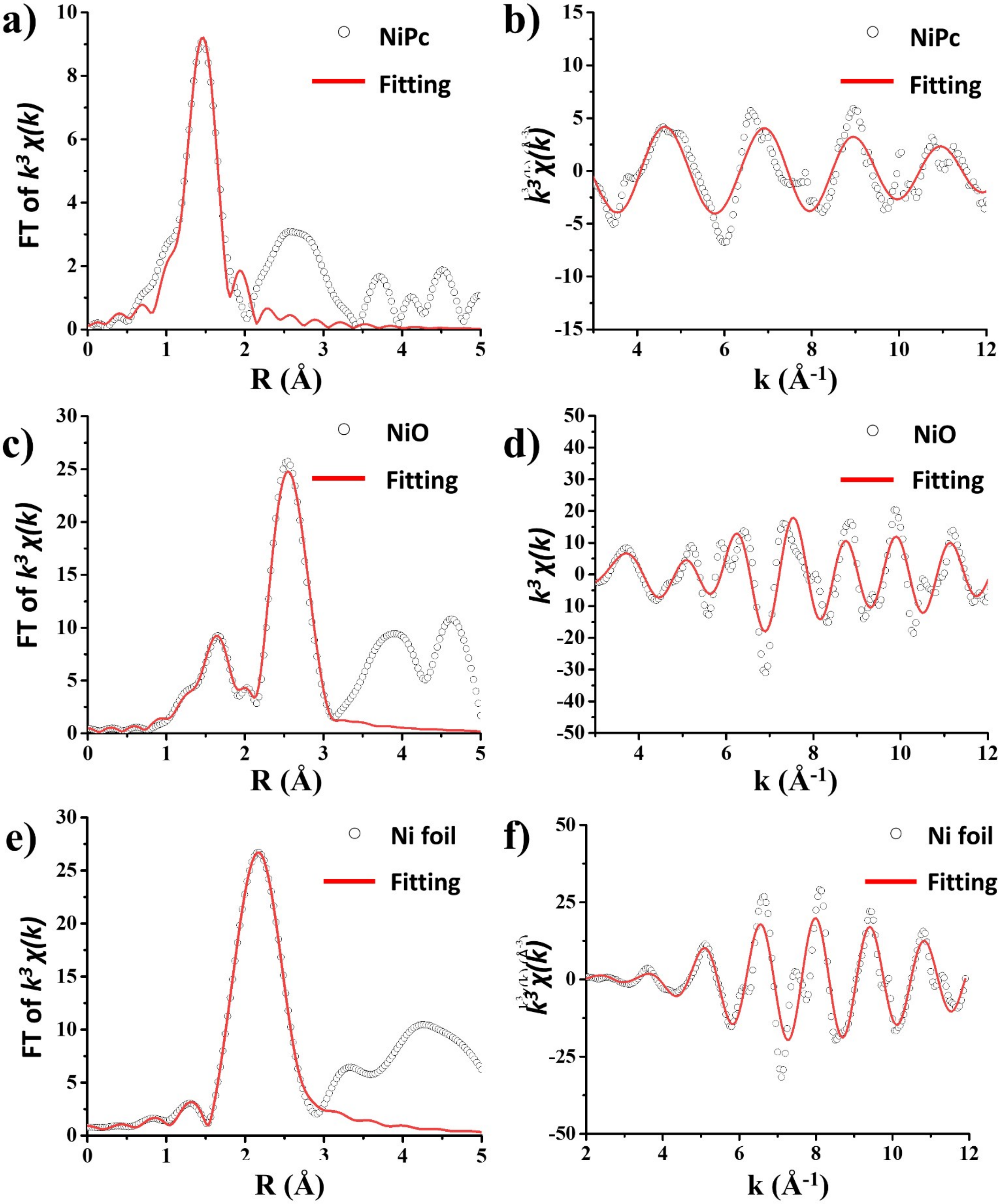

Figure S5. EXAFS fitting results of Ni K-edge in NiPc (nickel phthalocyanine), NiO and Ni foil.

Table S2. EXAFS fitting parameters at the Ni K-edge of various samples

Catalysts	**Path**	**Coordination numbers**	**R [a](Å)**	**σ^2 ($\times 10^{-3}$Å^2) [b]**	**ΔE_0 (eV) [c]**	**R factor [d]**
Ni_2/N-C	Ni-N	3.5 ± 1.0	2.04 ± 0.02	11.2 ± 3.5	-1.6 ± 2.9	0.010
Ni_1/N-C	Ni-N	4.0 ± 0.6	2.04 ± 0.01	8.3 ± 1.8	-2.3 ± 1.7	0.007
Ni foil	Ni-Ni	12 [e]	2.48 ± 0.01	6.1 ± 0.4	6.8 ± 0.5	0.001
NiPc	Ni-N	4.5 ± 0.9	1.88 ± 0.001	4.0 ± 1.7	2.9 ± 2.6	0.019
NiO	Ni-O	6.2 ± 1.2	2.08 ± 0.01	4.6 ± 1.7	-4.7 ± 2.4	0.005
	Ni-Ni	14.1 ± 1.7	2.95 ± 0.01	6.8 ± 0.7	-6.7 ± 1.1	

[a] *R*: bond distance; [b] σ^2: Debye-Waller factors (a measure of thermal and static disorder in absorber-scatterer distances); [c] ΔE_0: the inner potential correction (the difference between the zero kinetic energy value of the sample and that of the theoretical model); [d] *R* factor: goodness of fit. [e] the experimental EXAFS fit of metal foil by fixing coordination numbers as the known crystallographic value.

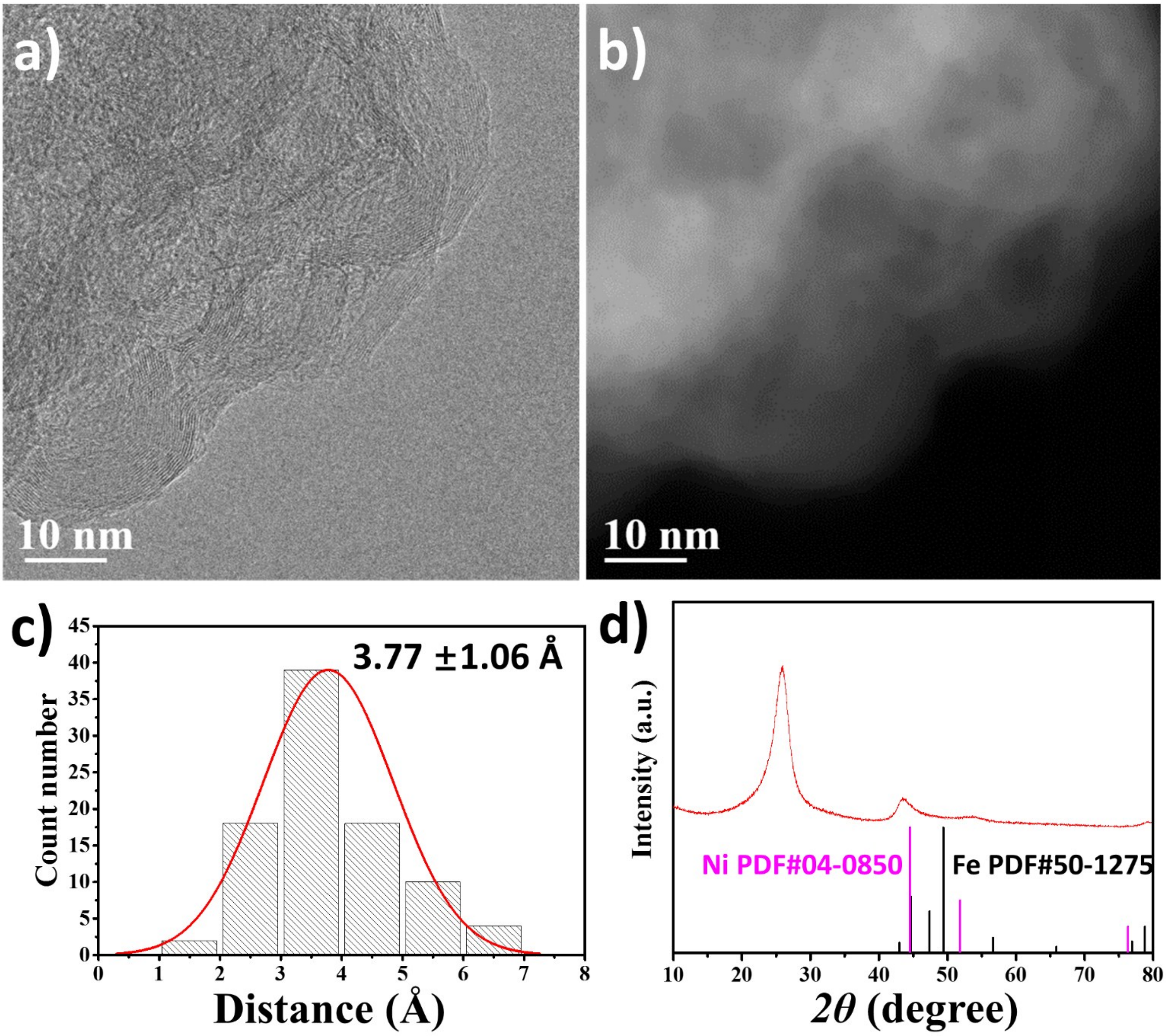

Figure S6. (a) TEM image; (b) STEM image; (c) the average distances of pairwise Fe_1/Ni_1 atoms and their distributions by averaging at least 60 pairs of Fe_1 and Ni_1 atoms randomly distributed in the ac HAADF-STEM images; (d) PXRD patterns of Fe_1Ni_1/N-C.

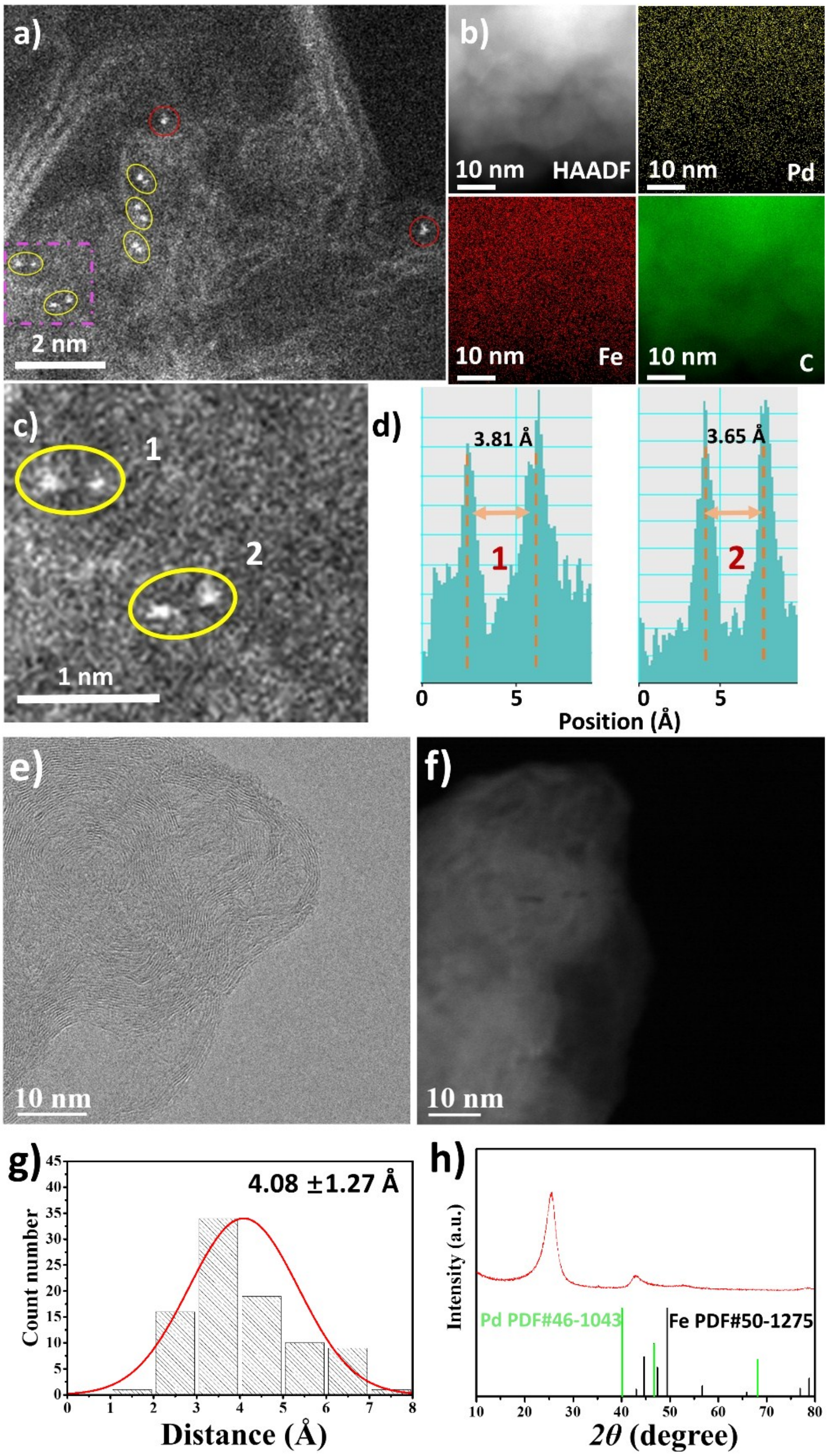

Figure S7. (a) ac HAADF-STEM of Fe_1Pd_1/N-C and fragmented M_1/N-C (M_1 = Fe or Pd) were marked with yellow and red circles, respectively; (b) HAADF-STEM image, and corresponding element maps showing well distributions of Fe (red), Pd (yellow), C (green), respectively; (c) partially expanded ac HAADF-STEM image of (a); (d) intensity profiles obtained in areas labeled 1 and 2 in (c); (e) TEM image; (f) STEM image; (g) the average distances of pairwise Fe_1/Pd_1 atoms and their distributions by averaging at least 30 pairs of Fe_1Pd_1 atoms randomly distributed in the ac HAADF-STEM images; (h) PXRD patterns of Fe_1Pd_1/N-C.

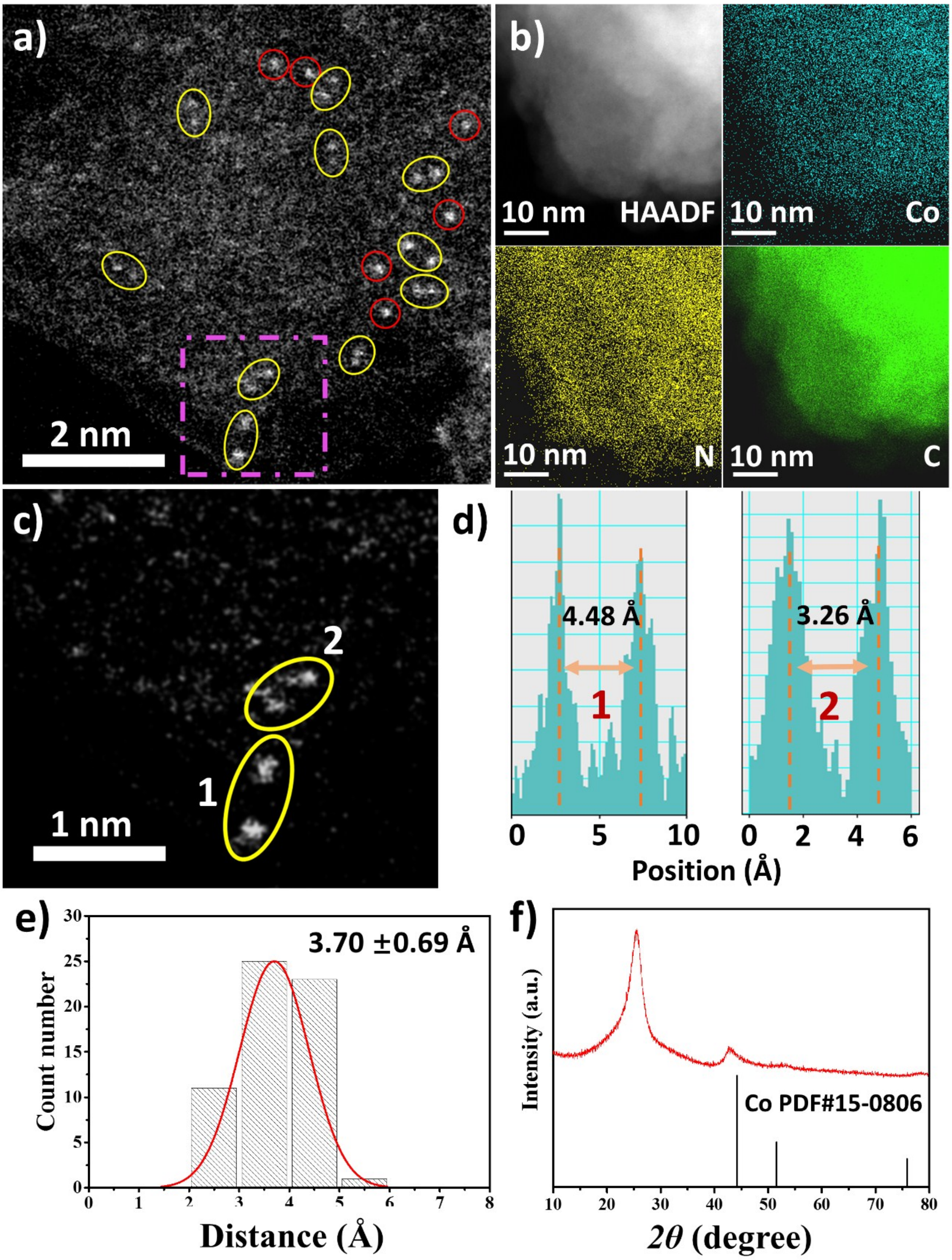

Figure S8. (a) ac HAADF-STEM of Co_2/N-C and fragmented Co_1/N-C were marked with yellow and red circles, respectively; (b) HAADF-STEM image, and corresponding element maps showing well distributions of Co (cyan), N (yellow), C (green), respectively; (c) partially expanded ac HAADF-STEM image of (a); (d) intensity profiles obtained in areas labeled 1 and 2 in (c); (e) the average distances of pairwise Co atoms and their distributions by averaging at least 60 pairs of Co atoms randomly distributed in the ac HAADF-STEM images ; (h) PXRD patterns of Co_2/N-C.

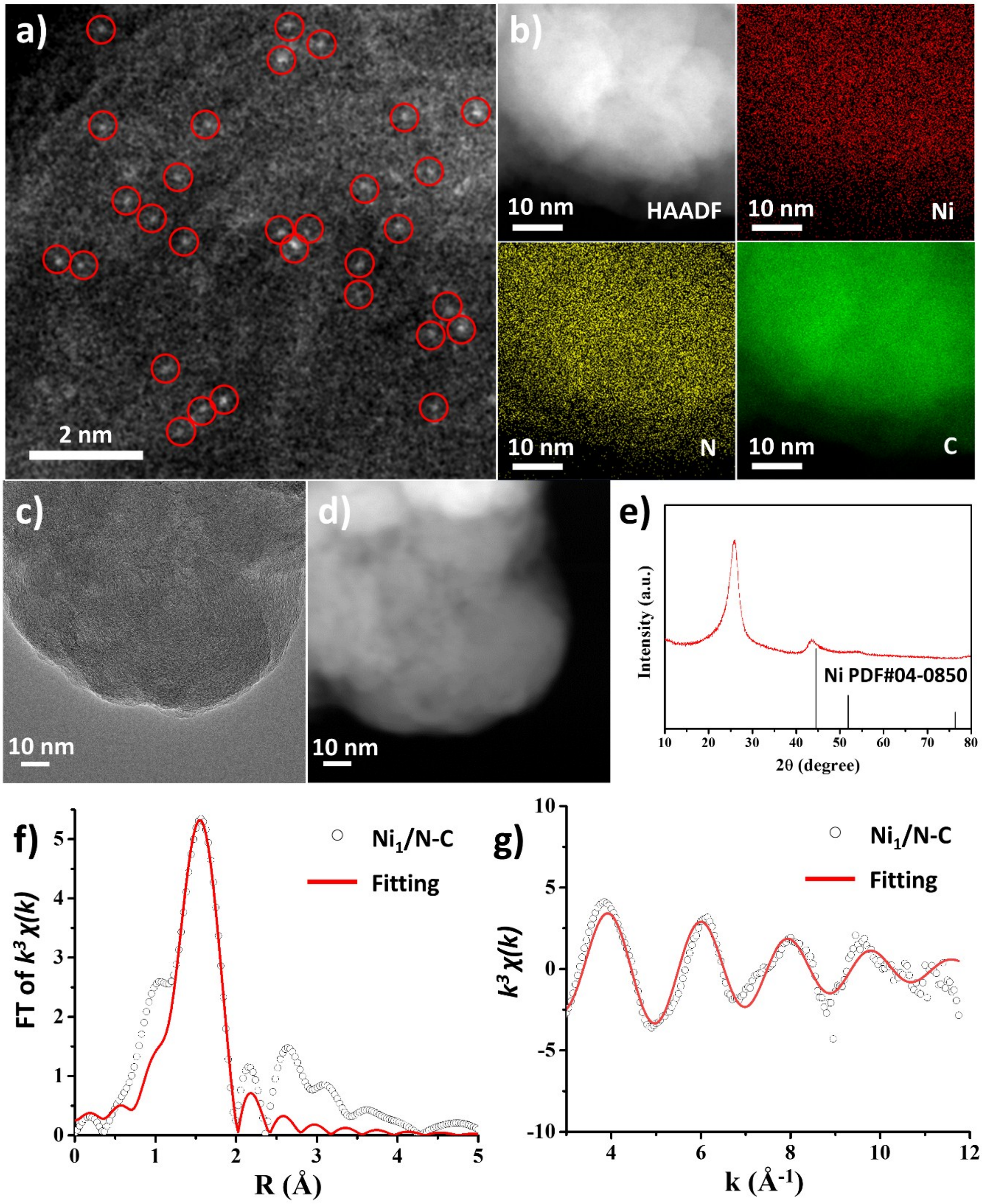

Figure S9. (a) ac HAADF-STEM of single-atom Ni$_1$/N-C was marked with red circles; (b) HAADF-STEM image, and corresponding element maps showing well distributions of Ni (red), N (yellow), C (green), respectively; (c) TEM image; (d) STEM image; (e) PXRD patterns of Ni$_1$/N-C. (g, h) EXAFS fitting results of Ni K-edge at R and k space in Ni$_1$/N-C, respectively;

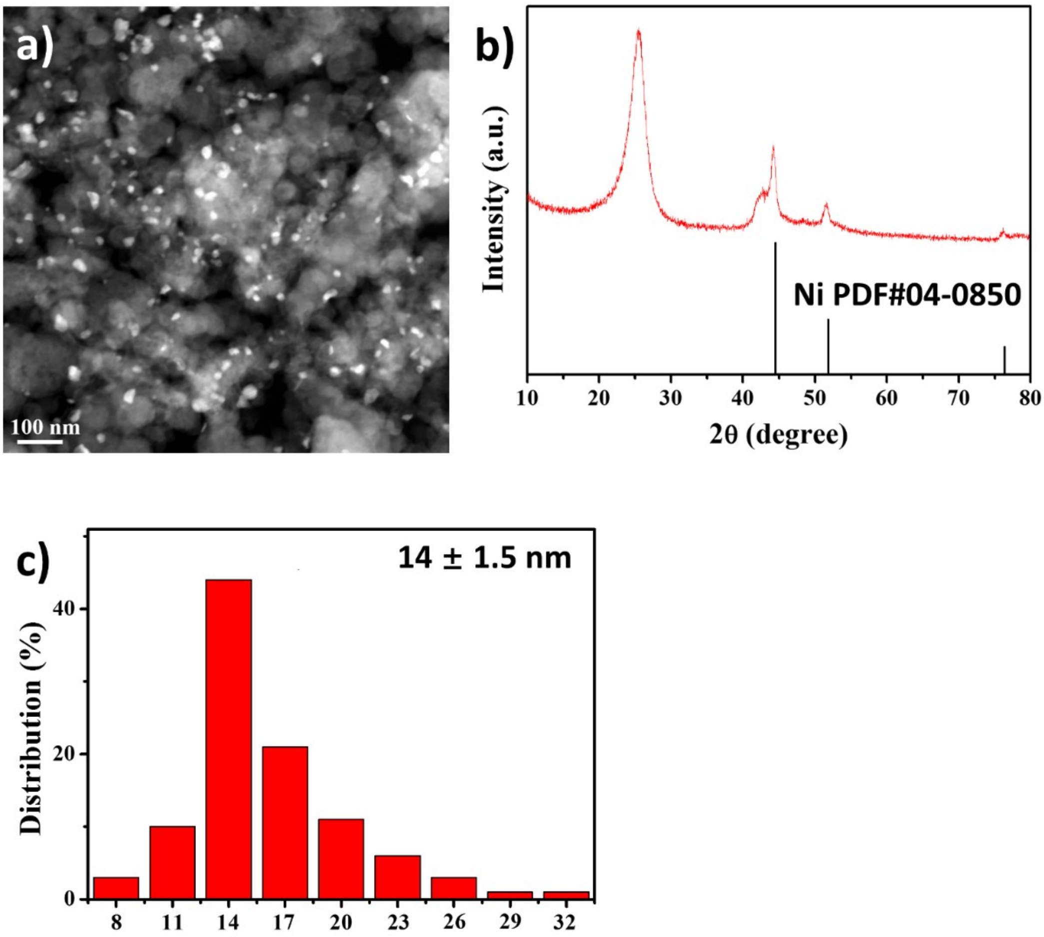

Figure S10. (a) STEM image; (b) PXRD patterns; (c) the average sizes of Ni nanoparticles and their distributions by averaging at least 100 particles randomly distributed in the STEM images.

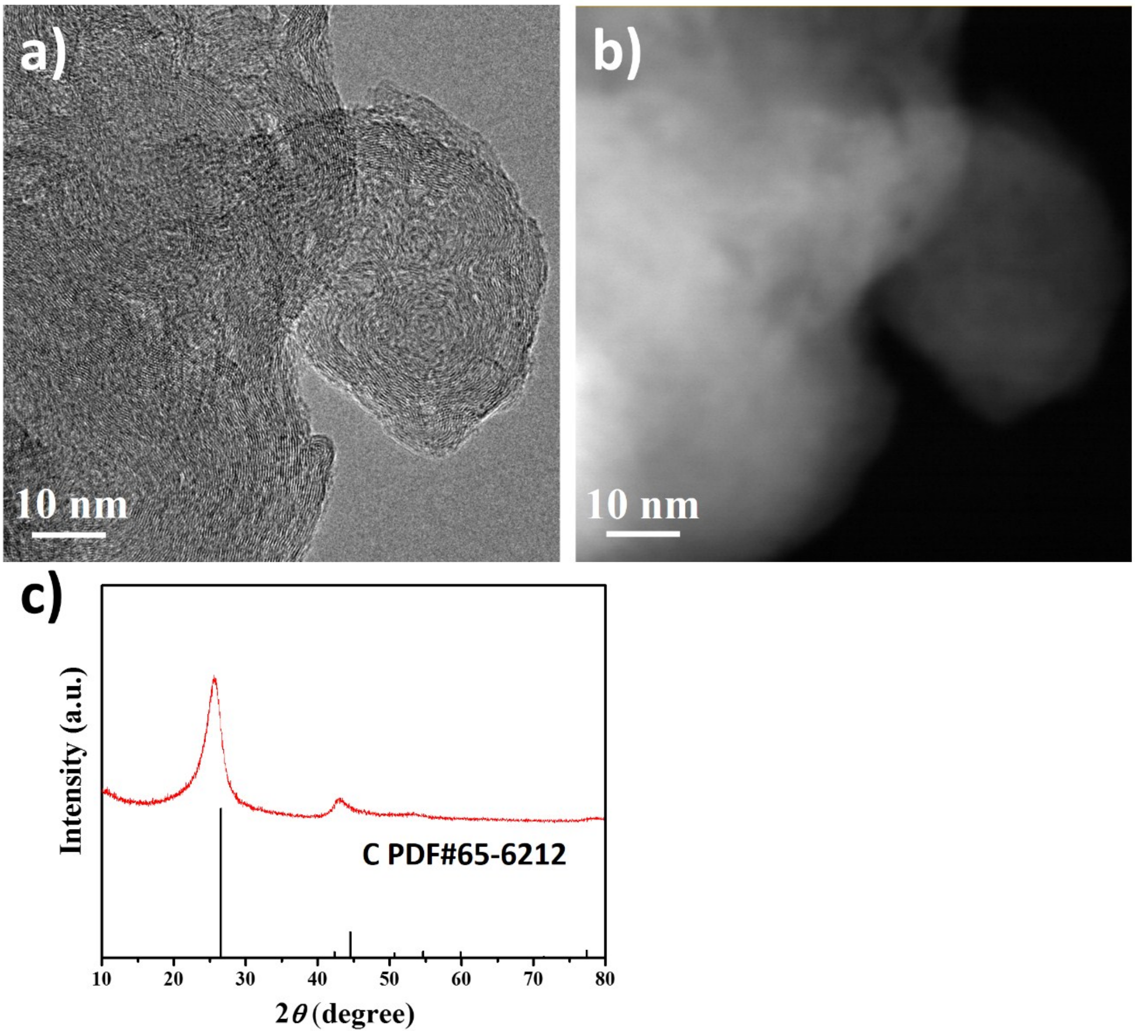

Figure S11. (a) TEM image; (b) STEM image; (c) PXRD patterns of the reference catalyst N-C.

Typical experimental procedure for r-WGS reaction

Catalytic tests of r-WGS reaction were carried out in a vertical continuous-flow fixed-bed quartz reactor with inner diameter of 7 mm at atmospheric pressure. About 100 mg powders of catalysts were held at the center of the reactor with quartz-wool plugs and running under differential reactor conditions with the effluent quantified by online gas chromatography with a molecular sieve (TDX-01) packed column and thermal conductivity detector (TCD). The total reactant flow rate in all studies was 45 standard cm^3 per minute (sccm). Gases were delivered via Teledyne mass flow controllers. The $H_2 : CO_2$ ratio was varied from 10:1 to H_2-lean conditions, 1:1, by varying individual flow rates. Inert He carrier gas was used at all conditions with a flow rate of 34.3 sccm. It is important to note that for each reaction condition a fresh sample was loaded into the reactor to ensure each experiment was measuring the reactivity of freshly prepared samples. Reaction rates and selectivity were calculated by averaging three measurements taken during the first hour on stream. See Table S2 for experimental details regarding reactant flow rates for each condition.

The activity values of catalysts were normalized on the basis of the weight of Ni:

$$\text{Activity} = \frac{F_{CO_2} X_{CO_2} M}{WP}$$

where F_{CO2} denotes the molar number of CO_2 molecules at the reaction temperature per unit time ($mol \cdot s^{-1}$), X_{CO2} denotes the conversion of CO_2 molecules by comparison of its outflow and inflow [S9], M is the atomic mass of Ni ($g \cdot mol^{-1}$), W denotes the weight of the catalyst packed into the reactor (g), and P denotes the loading amount of Ni in the catalysts.

Table S3. Reactant flow rates in packed bed reactor experiments

Gas (sccm)	**$H_2: CO_2$**	**$2H_2: CO_2$**	**$4H_2: CO_2$**	**$10H_2: CO_2$**
CO_2	7.5	4.0	2.1	0.9
H_2	7.5	8.0	8.6	8.8
He	30.0	32.0	34.3	35.3

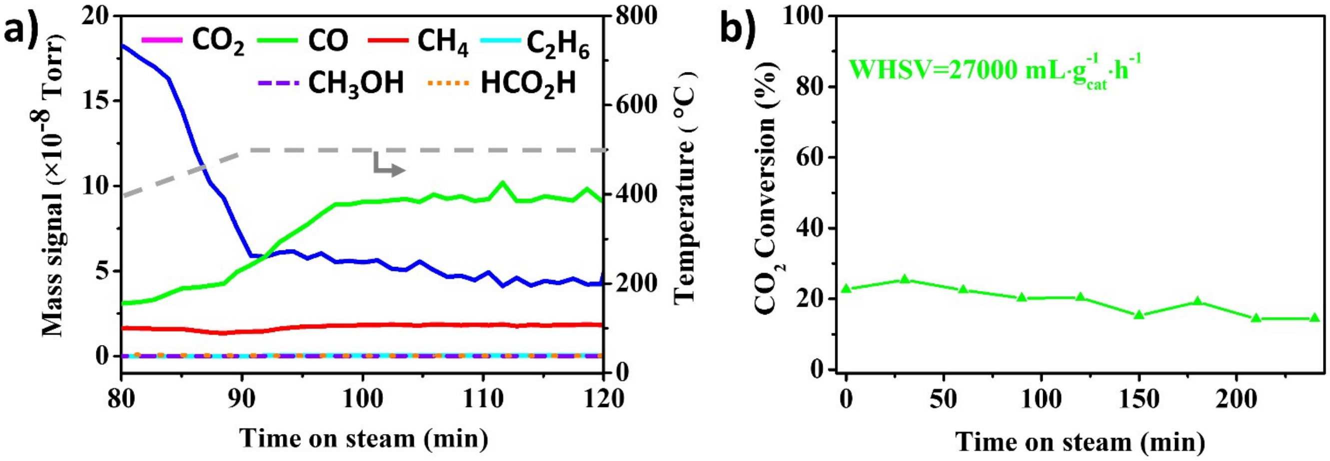

Figure S12. a) Mass spectrometry traces or r-WGS reactions catalyzed by Ni_2/N-C and b) the catalytic stability of Ni_2/N-C at 773 K and the weight hourly space velocity of 27000 mL·g_{cat}^{-1}·h^{-1} with the $4H_2$: $1CO_2$ feed ratio.

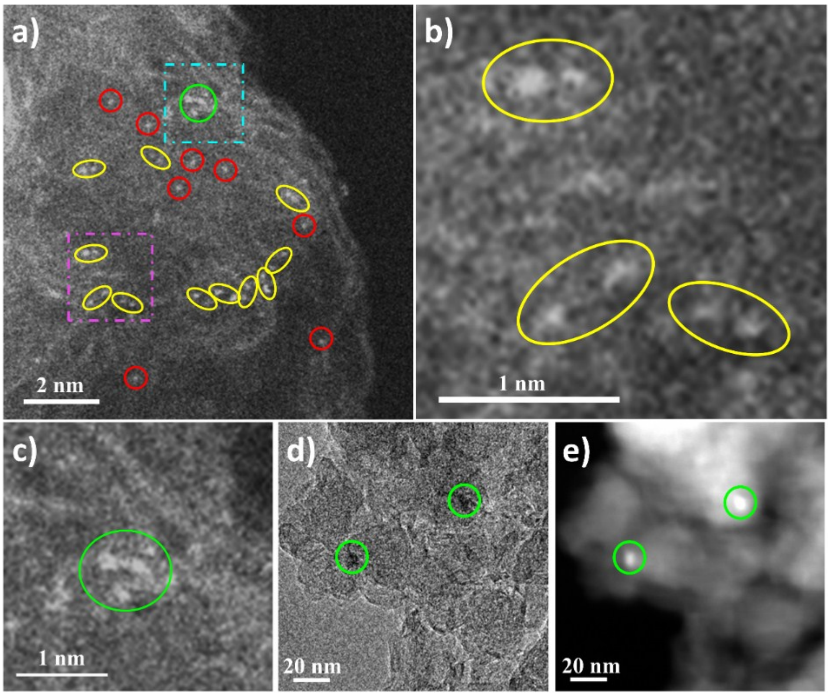

Figure S13. a) ac HAADF-STEM of recycled Ni_2/N-C catalyst, in which Ni_2/N-C, fragmented Ni_1/N-C and probable Ni nanocluster were marked with yellow, red and green circles, respectively; b-c) partially expanded ac HAADF-STEM images of (a); d-e) TEM and STEM images of the recycled Ni_2/N-C.

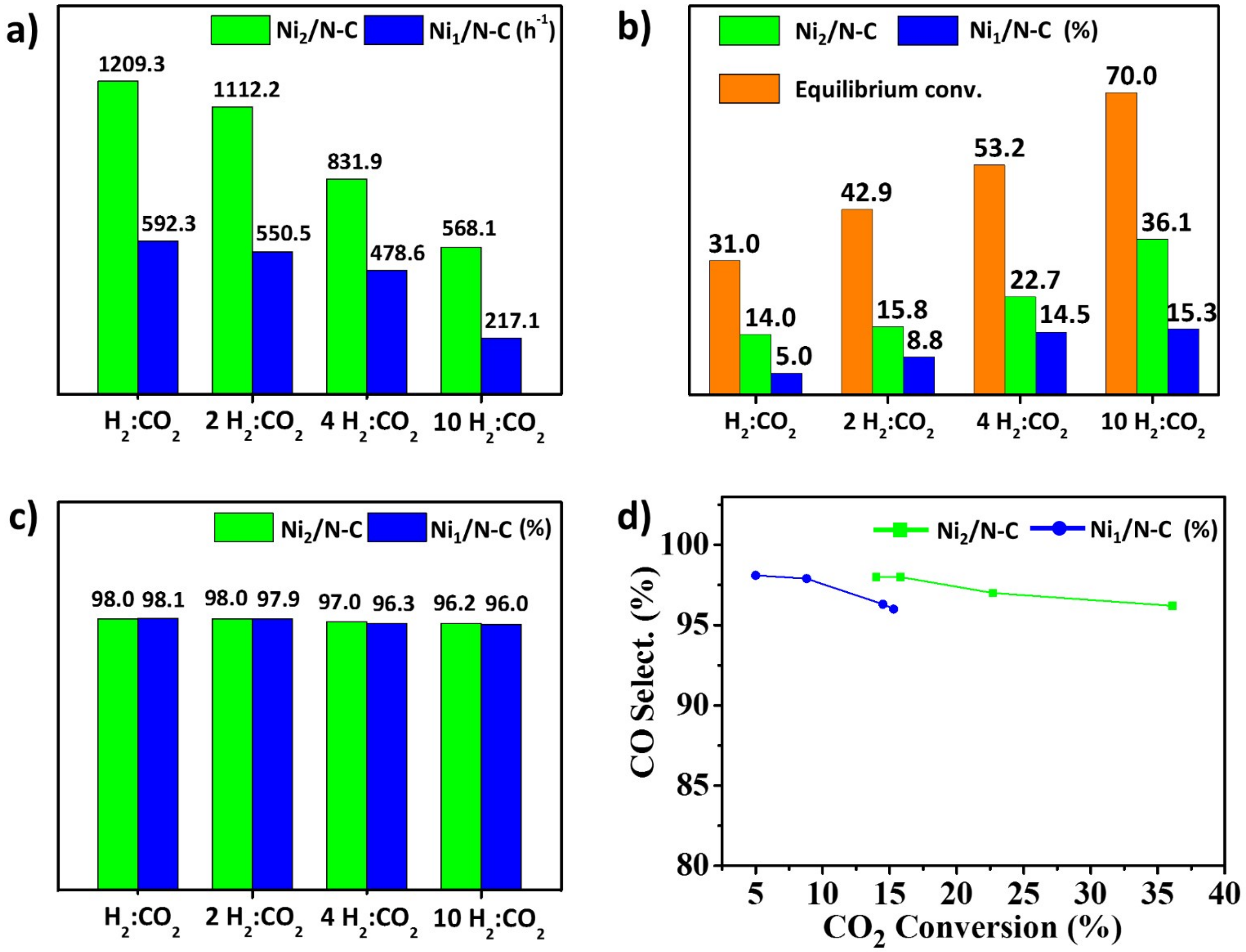

Figure S14. a) Activity (h^{-1}), b) CO_2 conversion (%), c) CO selectivity (%) and d) CO selectivity as a function of CO_2 conversions for the r-WGS reactions catalyzed by Ni_2/N-C and Ni_1/N-C at 773 K and the weight hourly space velocity of 27000 $mL \cdot g_{cat}^{-1} \cdot h^{-1}$ under varying H_2/CO_2 feed ratios.

Typical experimental procedure for H_2-D_2 exchange experiments of catalysts

H_2-D_2 exchange experiments of Ni_2/N-C and Ni_1/N-C were carried out in a vertical continuous-flow fixed-bed quartz reactor with inner diameter of 7 mm at atmospheric pressure. About 5 mg powders of catalysts were held at the center of the reactor with quartz-wool plugs. The flow rates of 20% H_2/Ar purging of the sample tube in all studies were kept at 10 standard cm^3 per minute. After the temperature stabilizing at 773 K, the sample was dosed with D_2 by 100 μL STP pulses, in 5 min intervals. And the proportions of HD (m/z = 3) were quantified by online mass spectrometry (Hiden Analytical HPR-20 QIC benchtop Gas Analysis System). The conversions of D_2 were obtained by averaging three doses at about 10 mins intervals.

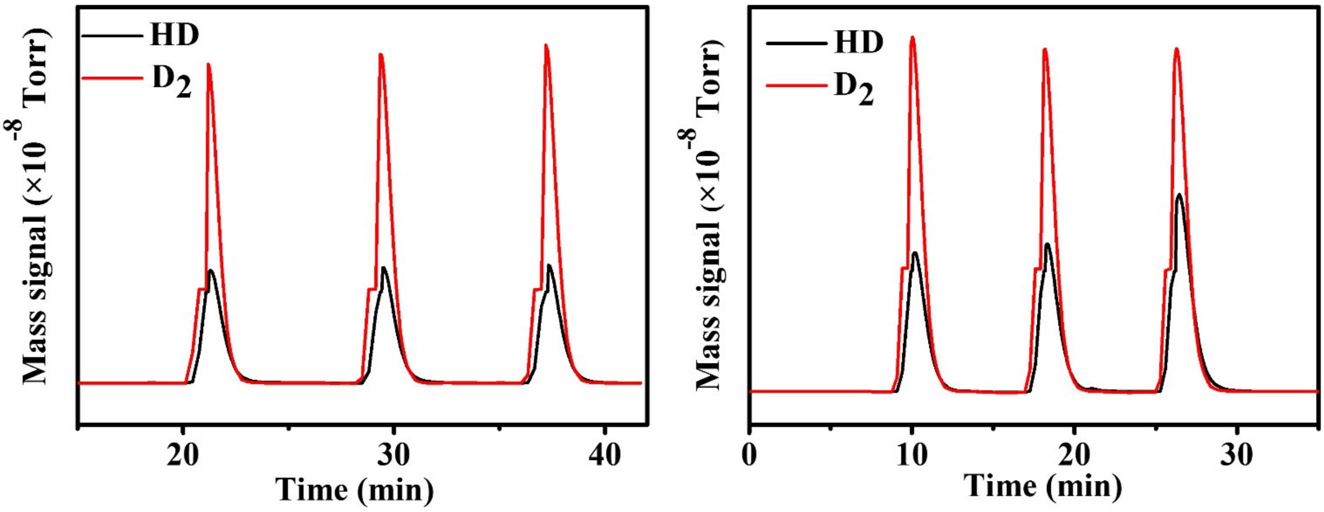

Figure S15. H_2-D_2 exchange experiments of Ni_2/N-C (left) and Ni_1/N-C (right) at 773 K, which showed 18.1 % and 24.3 % conversions, respectively, by mass spectrometry traces of HD (black, m/z = 3) and D_2 (red, m/z = 4), indicating no obvious difference for activation of hydrogen gas.

Table S4. The reported catalysts for r-WGS reaction

Catalyst	Metal loading (wt.%)	H_2/CO_2 feed ratio	T (K)	P (bar)	Selectivity (%)			Convern. (%)	Activity (h^{-1})	Ref.
					CO	CH_4	C_{2+}			
Ni_2/N-C	0.09	4	773	1	97.0	3.0	0	22.7	831.9	This work
Ni_2/N-C	0.09	1	773	1	98.0	2.0	0	14.0	1209.3	This work
Ni_1/N-C	0.1	4	773	1	96.3	3.7	0	14.5	478.6	This work
Pd/SiO_2	6.2	4	723	1	89.6	10.4	0	40.8	38.3	S7
Mg/SiO_2	6.2	4	723	1	89.7	10.3	0	0.8	0.2	S7
$Pd-Fe/SiO_2$	Pd (6.2), Fe (3.6)	4	723	1	97.2	2.8	0	44.7	11.8	S7
$Ru/mSiO_2$-N	0.4	4	673	1	93.4	6.6	0	13.7	457.2	S8
$LaFe_{0.5}Ni_{0.5}O_3$	Ni (12.0)	2	673	1	96.6	3.2	0.2	16.3	9.0	S9
Pt/TiO_2	2.0	1	673	1	88.0	12.0	0	21.0	403.2	S10
Pd/Fe_2O_3	0.1	4	673	1	77.5	0	22.5	3.9	1111.7	S11
Pd/Fe_2O_3	3.0	4	673	1	94.6	2.8	2.6	8.8	83.6	S11
Au/TiO_2	1.0	1	623	1	100	0	0	8.2	1152.0	S12

Reference

(S1) F. Möller, K. Merz, C. Herrmann and U.-P. Apfel, *Dalt. Trans.*, 2016, **45**, 904-907.

(S2) Y. Dussart, C. Harding, P. Dalgaard, C. McKenzie, R. Kadirvelraj, V. McKee and J. Nelson, *J. Chem. Soc. Dalt. Trans.*, 2002, 1704–1713.

(S3) M. Inosako, A. Kunishita, M. Kubo, T. Ogura, H. Sugimoto and S. Itoh, *Dalt. Trans.*, 2009, 9410.

(S4) O. V. Dolomanov, L. J. Bourhis, R. J. Gildea, J. A. K. Howard and H. Puschmann, *J. Appl. Crystallogr.*, 2009, 42, 339–341.

(S5) A. L. Spek, *J. Appl. Crystallogr.*, 2003, **36**, 7–13.

(S6) G. M. Sheldrick, *Acta Crystallogr. Sect. C Struct. Chem.*, 2015, **71**, 3–8.

(S7) J.-N. Park and E. W. McFarland, *J. Catal.*, 2009, **266**, 92–97

(S8) J. Dou, Y. Sheng, C. Choong, L. Chen and H. C. Zeng, *Appl. Catal. B Environ.*, 2017, **219**, 580–591.

(S9) B. Zhao, B. Yan, Z. Jiang, S. Yao, Z. Liu, Q. Wu, R. Ran, S. D. Senanayake, D. Weng and J. G. Chen, *Chem. Commun.*, 2018, **54**, 7354–7357.

(S10) X. Chen, X. Su, H. Duan, B. Liang, Y. Huang and T. Zhang, *Catal. Today*, 2017, **281**, 312–318.

(S11) F. J. Caparrós, L. Soler, M. D. Rossell, I. Angurell, L. Piccolo, O. Rossell and J. Llorca, *ChemCatChem*, 2018, **10**, 2365–2369.

(S12) X. Chen, X. Su, H.-Y. Su, X. Liu, S. Miao, Y. Zhao, K. Sun, Y. Huang and T. Zhang, *ACS Catal.*, 2017, **7**, 4613–4620.

NMR and ESI-HRMS spectra

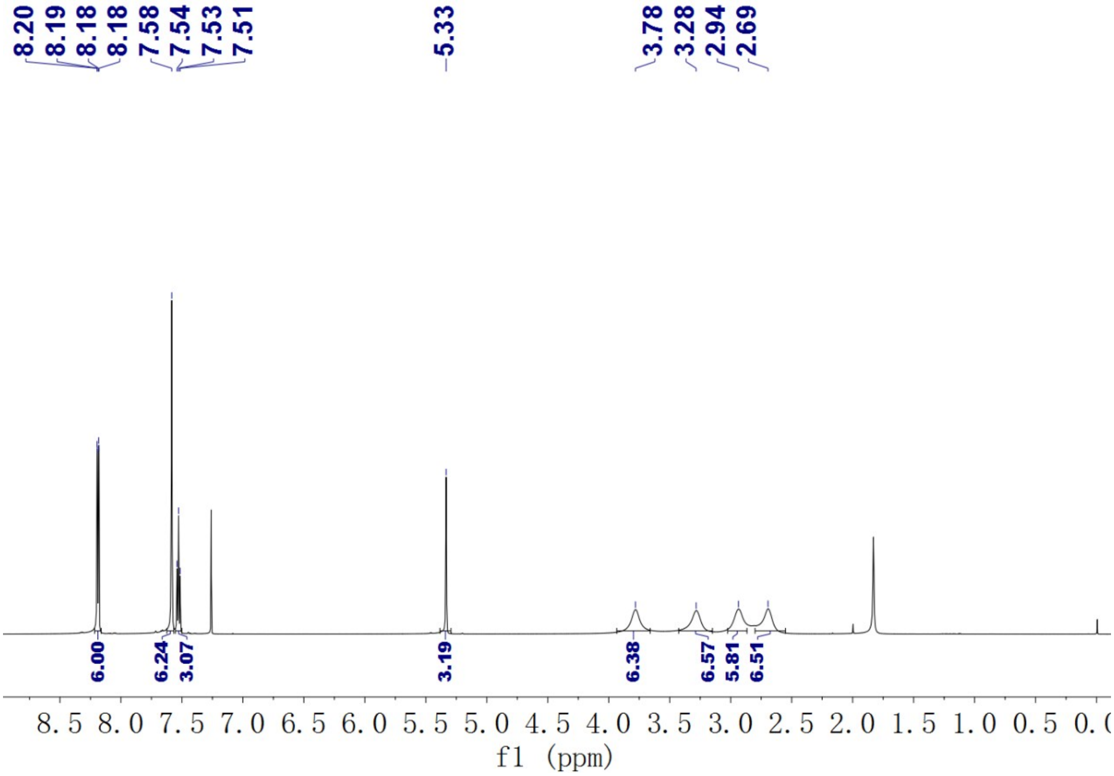

Figure S16. ^{1}H-NMR spectrum of Compound A in $CDCl_3$

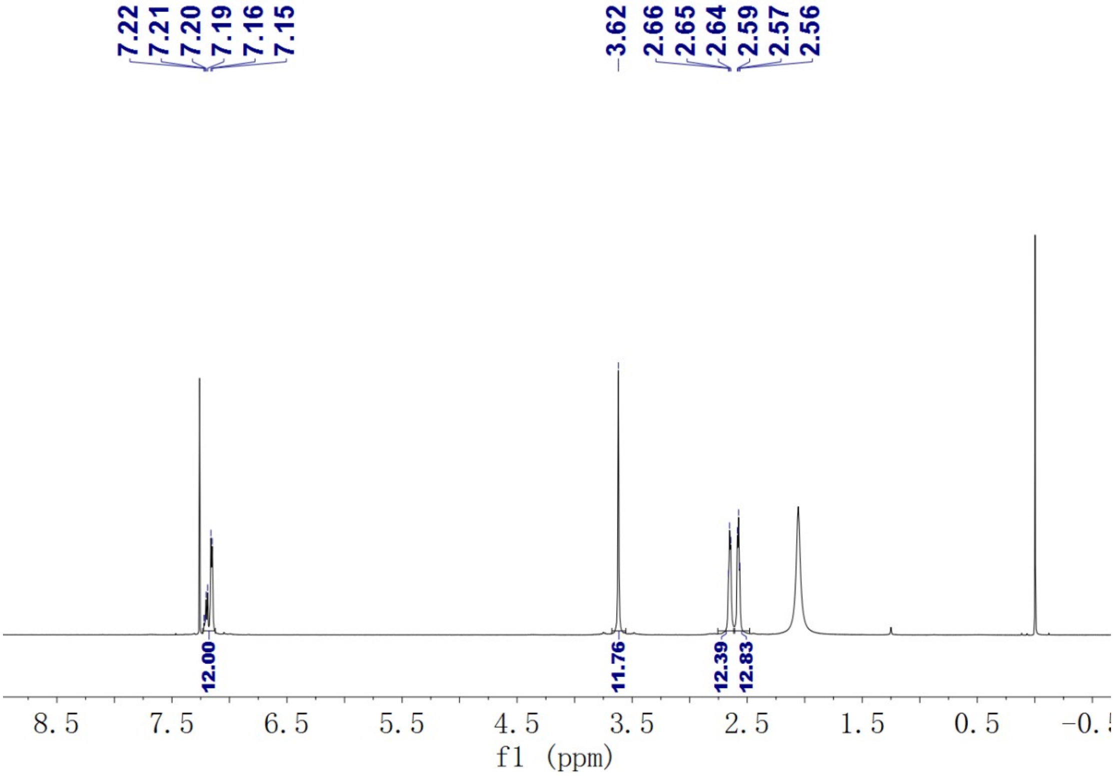

Figure S17. ^{1}H-NMR spectrum of Compound B in $CDCl_3$

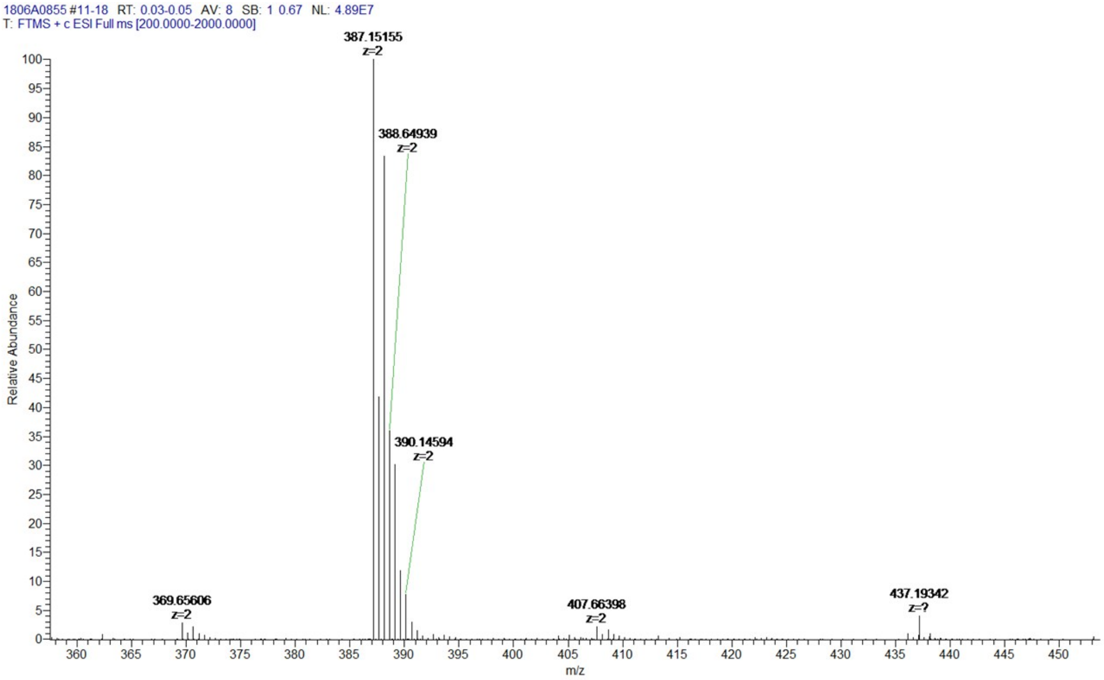

Figure S18. ESI-HRMS spectrum of dinuclear nickel cryptate

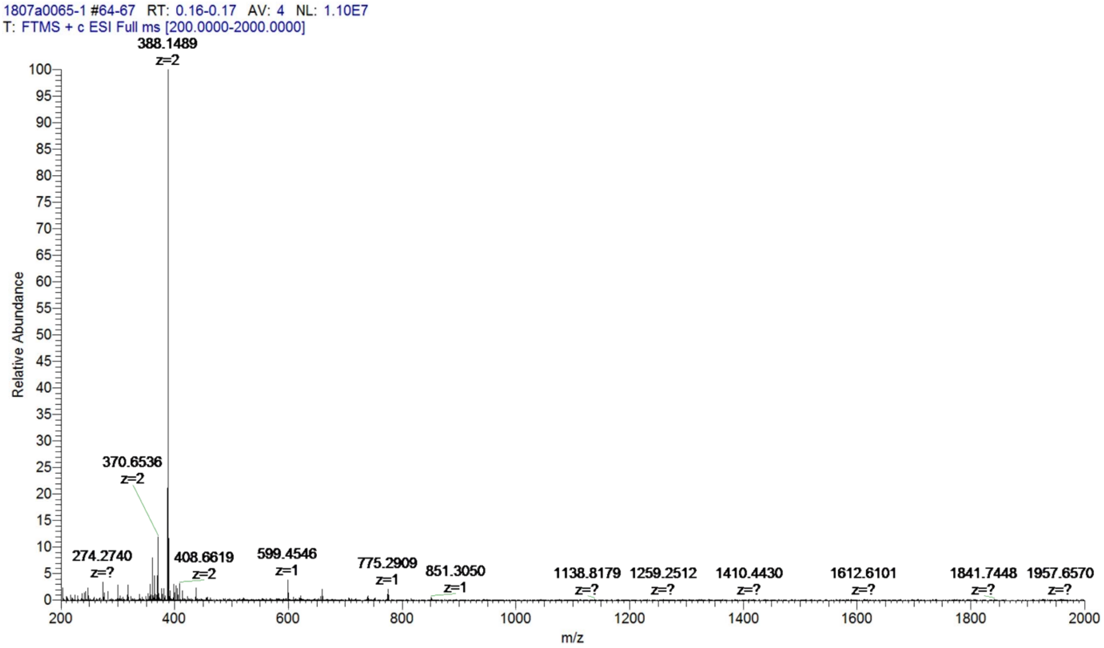

Figure S19. ESI-HRMS spectrum of dinuclear cobalt cryptate

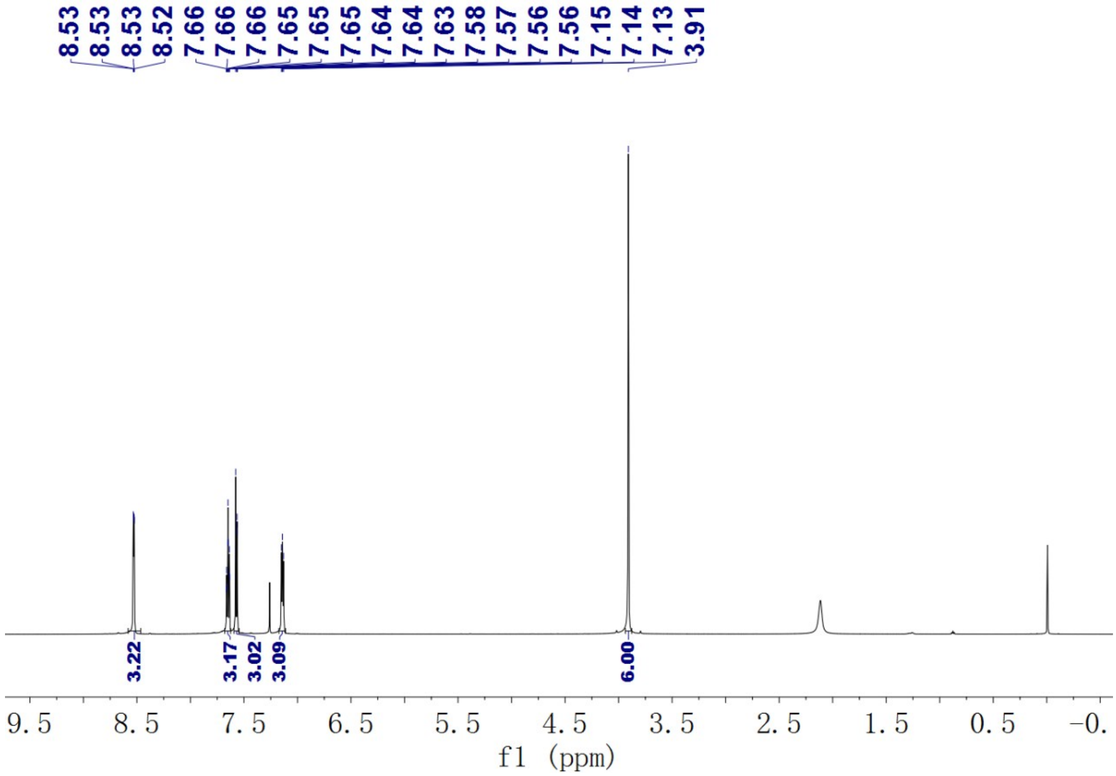

Figure S20. ^{1}H-NMR spectrum of tris(2-pyridyl)methylamine (TPA) in $CDCl_3$

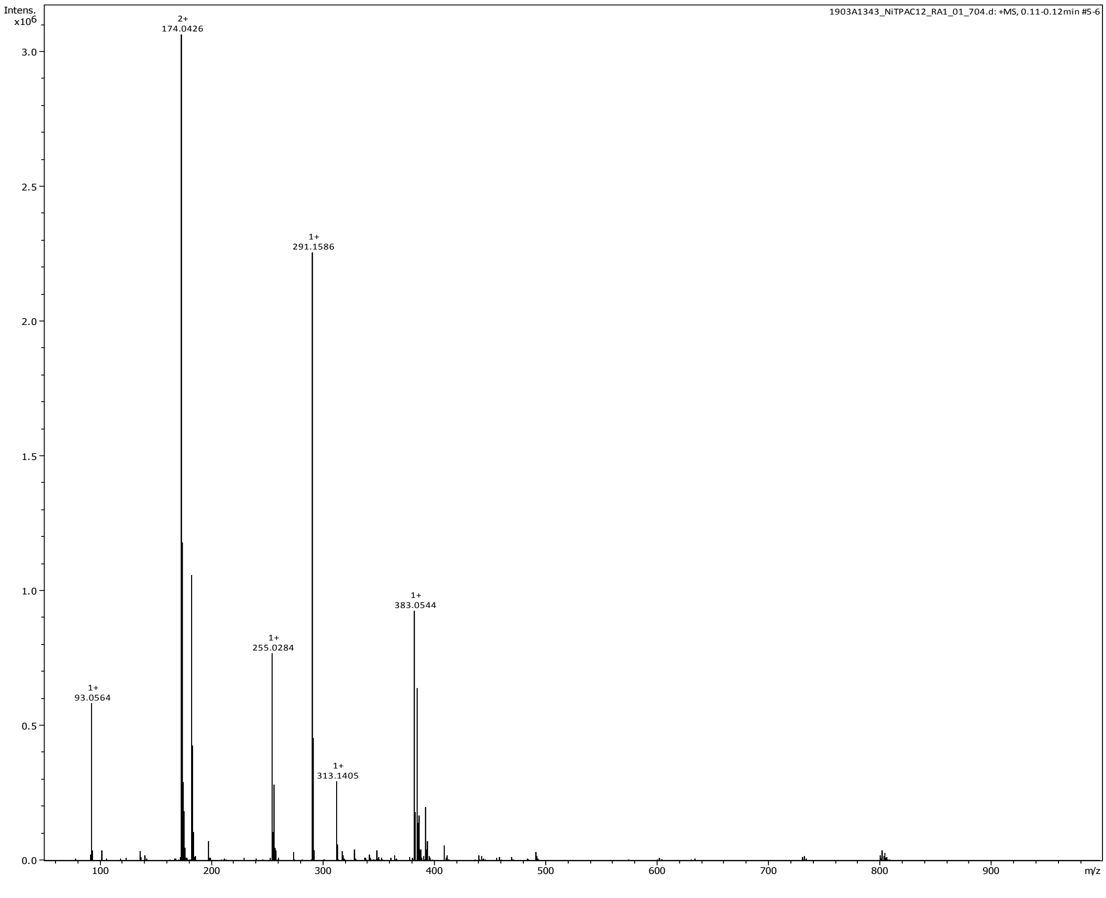

Figure S21. ESI-HRMS spectrum of $NiCl_2TPA$